INSTITUTE OF PHYSICS PUBLISHING JOURNAL OF PHYSICS: CONDENSED MATTER

J. Phys.: Condens. Matter **13** (2001) 7477–7498 PII: S0953-8984(01)24545-7

Introduction to x-ray scattering

Eberhard Burkel

Physics of New Materials, Department of Physics, University of Rostock, August-Bebel-Str.55, 18055 Rostock, Germany

E-mail: eberhard.burkel@physik.uni-rostock.de

Received 3 May 2001
Published 9 August 2001
Online at stacks.iop.org/JPhysCM/13/7477

Abstract

The basic knowledge needed for the performance and interpretation of scattering experiments is summarized. The probes for such experiments are x-rays and neutrons. The scattering mechanisms are discussed and applied to crystalline and non-crystalline materials for the determination of structural and dynamical properties.

1. Introduction

In condensed matter like crystalline, amorphous or liquid materials the atoms are located at distances of typically several ångströms. In order to resolve details of such structures in a scattering experiment, the wavelength λ of the scattering probe has to be of the same order of magnitude. For the determination of a lattice parameter a the wavelength λ has to obey $\lambda \leqslant a$.

Electromagnetic waves in the regime of x-rays with a typical energy of $E = h\nu = hc/\lambda =$ 10 keV have a wavelength of 1.24 Å. Thus, x-rays are well suited for structural investigations. X-rays couple to the electrons of the material.

Another probe suited for structural investigations are thermal neutrons. They are scattered by the nuclei in the material and interact with the electron spins. Due to their mass m_n the de Broglie wavelength of neutrons is $\lambda = h/\sqrt{2m_n E}$.

Thus, typical neutron energies of 50 meV correspond to a wavelength of 1.28 Å. Such neutrons are called thermal since their energies are of the same order as $k_B T_R \simeq 25$ meV with k_B being the Boltzman constant and $T_R = 300$ K the room temperature.

Electrons can also be used in scattering experiments. However, they show strong interactions with the electrons and the nuclei in the materials. Therefore, they experience only low penetration depths. For electrons with energies $E = 100$ eV and a mass m_e, the de Broglie wavelength corresponds to the wavelength $\lambda = 1.23$ Å.

Since x-rays are of central interest in this Euroschool, a brief discussion of their production follows.

1.1. Conventional x-ray xources

Classical sources for x-rays are generators where the x-rays are created in two different ways. High-energy electrons slowed down in an anode material give rise to radiation with a continuous frequency spectrum. This radiation is called bremsstrahlung. It is observed when any charged particle is either accelerated or decelerated. The total radiated power P of an accelerated electron was calculated by Larmor to be

$$P = \frac{2e^2}{3c^3}\left|\frac{\mathrm{d}\boldsymbol{v}}{\mathrm{d}t}\right|^2 \tag{1}$$

where $\boldsymbol{v}$ describes the velocity of the electron. The angular distribution of the radiated power is given by

$$\frac{\mathrm{d}P}{\mathrm{d}\Omega} = \frac{e^2}{4\pi c^3}\left(\frac{\mathrm{d}\boldsymbol{v}}{\mathrm{d}t}\right)^2 \sin^2\varphi \tag{2}$$

with φ being the angle between the vectors of acceleration and radiation propagation. This distribution has rotational symmetry.

The second process which can be used for x-ray generation is the recombination of electrons after creation of unoccupied states in the inner shells of atoms in the anode by collisions and/or photoionization. This recombination radiation is emitted as a sharp characteristic line with a wavelength determined by the transition energy between the corresponding shell levels.

The effectiveness of an x-ray tube is very low because less than 1% of the absorbed electron energy is emitted as x-ray radiation and the dominant part is converted to heat. Therefore, the x-ray intensity of conventional tubes is limited by the technical possibilities for the cooling of the anode. X-ray generators with water-cooled and rotating anodes allow working with electric powers of up to 90 kW.

1.2. Synchrotron radiation

Stronger sources for x-rays are nowadays synchrotrons and storage rings. The x-rays are contained in the radiation spectrum which is emitted by charged particles accelerated on circular orbits and which is called the synchrotron radiation spectrum.

Due to the high energy E_{el} of the particles, in the range of GeV, and the corresponding high velocity, close to the velocity of light ($v/c \approx 1$), the relativistic version of (1) has to be used to calculate the emitted radiation:

$$P \simeq \frac{2e^2c}{R^2}\left(\frac{v}{c}\right)^4\left(\frac{E_{\mathrm{el}}}{mc^2}\right)^4 \sim \frac{\gamma^4}{R^2} \tag{3}$$

where R is the radius of the storage ring or synchrotron and m is the rest mass of the particle. Due to the factor $(mc^2)^{-4}$ only electrons and positrons lead to strong radiation. The power of the emitted radiation is proportional to the fourth power of the reduced energy ($\gamma = E_{\mathrm{el}}/mc^2$). Therefore, with $mc^2 = 511$ keV for electrons, γ is of the order of 10^4.

The angular distribution of radiation for an accelerated charge in extreme relativistic motion is no longer described by the dipolar distribution of (2) and figure 1(a). The relativistic transformation causes a distortion of the radiation pattern in the direction of motion, as shown in figure 1(b). It becomes a narrow cone in the direction of the instantaneous velocity vector of the charge. Radiation will be visible only when the velocity of the electron is directed to the observer. It will be a burst of radiation, very short in time with $\Delta t \sim (R/c)\gamma^3$. The Fourier transform of this pulse shows a corresponding broad frequency spectrum of white radiation with a spectral cut-off just above the critical energy E_{c}, used to characterize the spectrum.

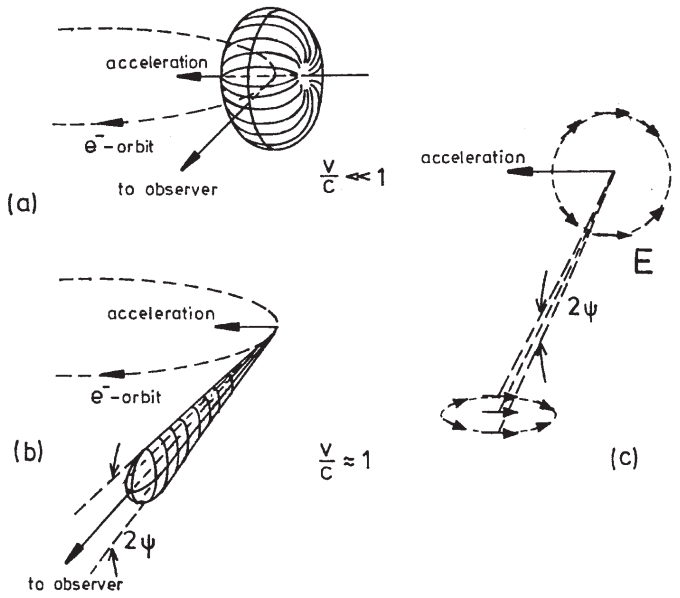

Figure 1. Radiation distribution for an electron for non-relativistic (a) and relativistic (b) motion on a circular orbit. (c) shows the far-field $\boldsymbol{E}$ distribution with the dipole characteristic in a plane vertical to the orbit plane. The distributions in the rest frame and after Lorentz transformation in the laboratory frame illustrate the polarization of the synchrotron radiation.

The horizontally moving electrons in a circular orbit can emit radiation at any point of the orbit within the bending magnets. Thus, the natural angular width of the radiation cone can only be observed in the vertical direction, leading to a vertical divergence of the photon beam. The horizontal angular width depends on the length of the observed arc (see also figure 1).

There is another important consequence of the relativistic motion of the electron or positron. The electric field $\boldsymbol{E}$ with its characteristic dipole distribution in the rest frame is contracted by the Lorentz transformation (figure 1(c)). As a consequence, the radiation is dominantly polarized with $\boldsymbol{E}$ in the plane of motion. As long as the radiation is observed within the orbit plane, it is completely linearly polarized. Observation at a small elevation angle ψ out of this plane will detect elliptically polarized radiation.

In straight sections of storage rings no radiation is emitted. However, the installation of periodic magnetic structures can lead to additional periodic deflections of the electron beam without disturbing the rest of the orbit. The induced oscillatory movements cause radiation. Its spectral and spatial behaviour is determined by the specific magnetic structure of such insertion devices.

Figures 2(b)–(d) indicate the electron beam trajectories and the radiation patterns for the insertion devices wavelength shifter, wiggler and undulator. For comparison, the radiation pattern for a bending magnet is given as well (figure 2(a)). In all cases the vertical angular width of the emitted radiation is of the order of $1/\gamma$. Only the horizontal angular width is varying.

A wavelength shifter (figure 2(b)) changes locally the radius of the electron path of a given storage ring. Because the power of radiation and its frequency distribution depend on the radius, their characteristics can be varied.

An undulator (figure 2(c)) is a spatial periodic arrangement of magnetic dipoles which leads to the emission of quasi-monochromatic radiation of relativistic electrons with a strongly

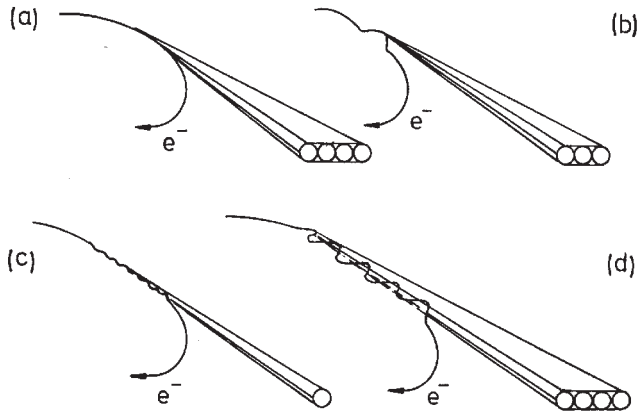

Figure 2. Beam trajectories and emission patterns for a bending magnet (a), wavelength shifter (b), undulator (c) and wiggler (d).

increased photon flux. The increased photon flux is due to a coherent superposition of wavelets emitted by each section of the undulator magnets. The dipole arrangement leading to such strong interference effects has to produce beam deflections which are always smaller than the opening angle $(1/\gamma)$ of the radiation. Therefore, the horizontal angular width of the radiation is about $1/\gamma$. The brightness of the radiation emitted by an undulator is greater than that of an ordinary bending magnet. This ratio is approximately the square of the number of periods. Due to the source size of small emittance rings the brilliance of the undulator is very high.

Periodic magnetic dipole arrangements leading to stronger deflections of the trajectory are called wigglers (figure 2(d)). Such multipole wigglers produce a complicated spectrum, which on the high-energy side resembles the simple addition of the spectra of several bending magnets. The brightness is increased by a factor corresponding to twice the number of periods. The horizontal opening angle and, therefore, the beam divergence is larger for the wiggler than for the undulator.

Special magnetic structures can also be defined to generate circularly polarized radiation.

Figure 3 shows the development of the brilliances of x-ray sources starting from conventional x-ray tubes and rotating anode x-ray generators. The different generations of synchrotron sources having bending magnets in the first generation, wigglers in the second and undulators in the third generation, led to an enormous increase in the brilliances. In particular, the very low emittance defined by the size and the angular divergence of the electron or positron beam circulating in the rings of the third generation sources contributed to these high values.

Still higher brilliances are expected to be achieved in the next, the fourth generation of x-ray sources (Brinkmann *et al* 1997) which are based on free electron lasers and use the concept of a single pass self-amplification of spontaneous emission (SASE), recently developed by Bonifacio *et al* (1994), Saldin *et al* (1995), Freund and Nai (1999) and Saldin *et al* (2000). During the path of an electron bunch through a long undulator structure, the interaction of the emitted synchrotron radiation and the propagating electromagnetic wave causes a density modulation of the travelling electron bunch. The electrons are sorted into microbunches which stimulates a self-amplifying emission of radiation. The saturation will be reached when all the microbunches radiate coherently. The emitted intensity of such a free electron laser device will then be proportional to the number of electrons squared leading to a peak brilliance up to ten orders of magnitudes higher than that presently achievable (figure 3).

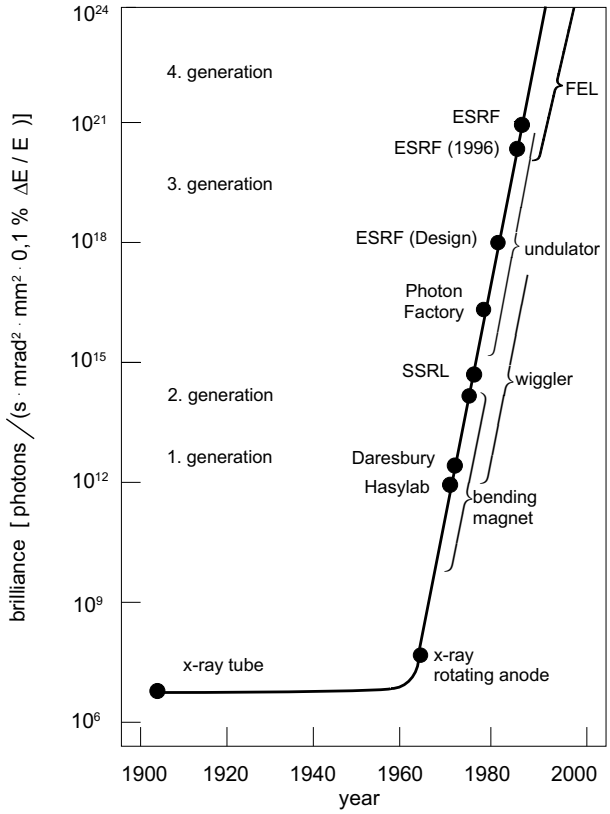

Figure 3. Brilliances of different x-ray sources given as the number of photons emitted in the unit time by the unit source area in the unit solid angle in a relative bandwidth of 10^{-3} for a certain photon energy.

2. Scattering cross section

A general scattering experiment is shown schematically in figure 4. This arrangement is valid for all probes such as neutrons, electron beams and electromagnetic radiation. The incident beam of well defined wavevector $\boldsymbol{k}_\mathrm{i}$, energy E_i and polarization unit vector $\boldsymbol{e}_\mathrm{i}$ is scattered into the solid angle element $\mathrm{d}\Omega$ under the scattering angles 2θ and ϕ. The scattered beam is completely defined by the new wavevector $\boldsymbol{k}_\mathrm{f}$, the energy E_f and the polarization unit vector $\boldsymbol{e}_\mathrm{f}$. $\boldsymbol{Q}$ is called the scattering vector. The scattered intensity is described by the double differential cross section $\mathrm{d}^2\sigma/(\mathrm{d}\Omega\,\mathrm{d}\omega_\mathrm{f})$. It is given by the removal rate of particles out of the incident beam as the result of being scattered into a solid angle $\mathrm{d}\Omega$ with a frequency range of $\mathrm{d}\omega_\mathrm{f}$ corresponding to an energy range $\mathrm{d}E_\mathrm{f} = \hbar\,\mathrm{d}\omega_\mathrm{f}$. This contains contributions of the beam that have been scattered elastically with no change of energy and other contributions that have changed energy due to inelastic scattering. Therefore, the scattering process contains information on energy and momentum transfers by

$$E = \hbar\omega \equiv E_\mathrm{i} - E_\mathrm{f} \tag{4}$$

and

$$\hbar\boldsymbol{Q} \equiv \hbar(\boldsymbol{k}_\mathrm{i} - \boldsymbol{k}_\mathrm{f}). \tag{5}$$

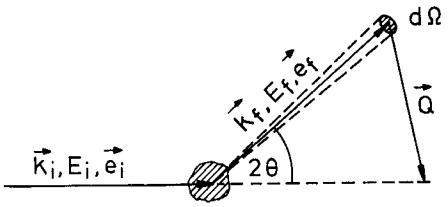

Figure 4. Scattering geometry

The discussion throughout this whole paper concentrates on the scattering of x-rays where the transferred energy is normally smaller than the photon energy ($E \ll E_\mathrm{i}$). In this case the momentum transfer $\hbar Q$ is simply connected with the scattering angle θ by

$$\hbar Q = 2\hbar k_\mathrm{i} \sin\theta. \tag{6}$$

There is a very elegant and informative presentation of the double differential scattering cross section,

$$\frac{\mathrm{d}^2\sigma}{\mathrm{d}\Omega\,\mathrm{d}\omega_\mathrm{f}} = \left(\frac{\mathrm{d}\sigma}{\mathrm{d}\Omega}\right)_0 S(\boldsymbol{Q}, \omega) \tag{7}$$

which was derived by Van Hove (1954). This description has the advantage of allowing us to separate the double differential cross section into two contributions. The coupling of the beam to the scattering system is characterized by the intrinsic cross section $(\mathrm{d}\sigma/\mathrm{d}\Omega)_0$ and the properties of the sample in the absence of the perturbing probe are expressed by the scattering function $S(\boldsymbol{Q}, \omega)$.

For the following, it is sufficient to concentrate on elastic scattering experiments with $E_\mathrm{i} = E_\mathrm{f}$ and to discuss the static scattering function $S(\boldsymbol{Q})$ and the single differential scattering cross section, $\mathrm{d}\sigma/\mathrm{d}\Omega$. In this case (7) can be rewritten,

$$\frac{\mathrm{d}\sigma}{\mathrm{d}\Omega} = \left(\frac{\mathrm{d}\sigma}{\mathrm{d}\Omega}\right)_0 S(\boldsymbol{Q}). \tag{8}$$

Inelastic scattering experiments will be treated in section 6.

A plane wave $\mathrm{e}^{\mathrm{i}\boldsymbol{k}_i\cdot\boldsymbol{r}}$ with wavevector $\boldsymbol{k}_\mathrm{i}$ is elastically scattered at a scattering centre at the fixed position $\boldsymbol{r} = \boldsymbol{0}$ (figure 5). At large distances from the scattering centre

$$\mathrm{e}^{\mathrm{i}\boldsymbol{k}_\mathrm{i}\cdot\boldsymbol{r}} \longrightarrow \mathrm{e}^{\mathrm{i}\boldsymbol{k}_\mathrm{i}\cdot\boldsymbol{r}} + f(\Omega)\frac{\mathrm{e}^{\mathrm{i}\boldsymbol{k}_\mathrm{f}\cdot\boldsymbol{r}}}{r} \tag{9}$$

holds. After the scattering process the original plane wave is superimposed by a spherical wave with the scattering amplitude $f(\Omega)$ called the *scattering length* due to its dimension of length.

The scattering intensity is then given by the differential cross section through

$$\left(\frac{\mathrm{d}\sigma}{\mathrm{d}\Omega}\right)_0 = |f(\Omega)|^2. \tag{10}$$

The total cross section taking into account all scattered particles is given by

$$\sigma = \int \left(\frac{\mathrm{d}\sigma}{\mathrm{d}\Omega}\right)_0 \mathrm{d}\Omega = \int_0^{2\pi} \mathrm{d}\phi \int_0^{\pi} \sin\theta\,\mathrm{d}\theta |f(\theta, \phi)|^2. \tag{11}$$

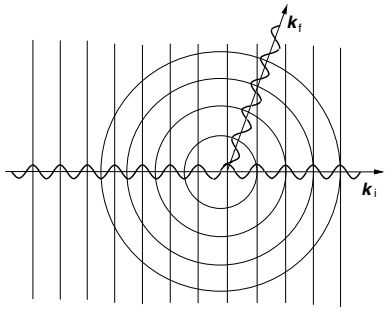

Figure 5. Scattering of a plane wave at a scattering centre at fixed position.

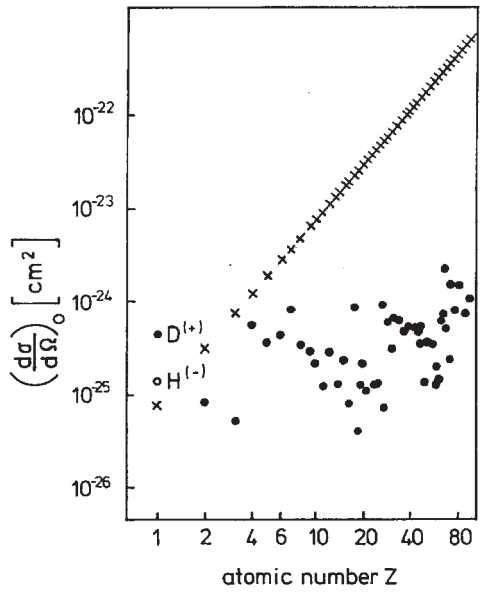

Figure 6. Intrinsic cross sections for coherent scattering of neutrons (•, ○) and for x-ray scattering (×) from atoms of the atomic number Z, in the forward direction ($Q \to 0$).

2.1. Neutron scattering by a fixed nucleus

The scattering length b of a nucleus is determined experimentally from the isotropic scattering cross section (figure 6)

$$\left(\frac{d\sigma}{d\Omega}\right)_0 = |b^2| = \text{constant}. \tag{12}$$

In general, the scattering length is a complex quantity which is characteristic for each nucleus. It is of the order of $|b| \sim 5 \times 10^{-15}$ m. The total scattering cross section is $\sigma = 4\pi|b^2|$. The scattering properties of neutrons are determined by the nucleus–nucleus interactions which are of short range ($\sim 10^{-15}$ m) compared to the large wavelength of the neutrons themselves ($\lambda_n \gg |b|$). They can be described by using so called *Fermi pseudo-potentials*. Due to different phase shifts during the scattering processes the scattering lengths can be positive or negative (see also Lovesey (1986)).

2.2. Scattering of electromagnetic radiation by a bound electron

A classical localized electron bound elastically to a fixed nucleus is hit by an electromagnetic wave. The electric field of this wave is described by

$$\boldsymbol{E}(\boldsymbol{r}, t) = \boldsymbol{e}_\mathrm{i} E_\mathrm{i}\, \mathrm{e}^{\mathrm{i}(\boldsymbol{k}_\mathrm{i}\cdot\boldsymbol{r}-\omega t)}. \tag{13}$$

$\boldsymbol{e}_\mathrm{i}$ is the polarization vector, and due to the transverse character of the wave, $\boldsymbol{e}_\mathrm{i}\cdot\boldsymbol{k}_\mathrm{i} = 0$ holds. The electric field of this wave excites the electron (mass m_e) into forced dipole oscillations. The equation of the motion $\boldsymbol{s}(t)$ for such an oscillator model can be written according to Newton as

$$m_\mathrm{e}\ddot{\boldsymbol{s}} + m_e\omega_\mathrm{r}^2\boldsymbol{s} - m_\mathrm{e}\gamma\dot{\boldsymbol{s}} = e\boldsymbol{E}(t) \tag{14}$$

assuming an eigenfrequency ω_r of the electron and a damping constant γ. The solution is

$$\boldsymbol{s}(t) = \frac{e}{m_\mathrm{e}}\frac{1}{\omega_\mathrm{r}^2 - \omega^2 - \mathrm{i}\gamma\omega}\cdot\boldsymbol{E}(t) \tag{15}$$

describing the forced damped oscillations of the electron. This induces an electric dipole moment

$$\boldsymbol{p}(t) = e\boldsymbol{s}(t) = \alpha(\omega)\boldsymbol{E}(t) \tag{16}$$

with the polarizability

$$\alpha(\omega) = \frac{e^2}{m_\mathrm{e}}\frac{1}{\omega_\mathrm{r}^2 - \omega^2 - \mathrm{i}\gamma\omega}. \tag{17}$$

However, an oscillating dipole itself acts as an emitter of an electromagnetic field leading to an electric field $\boldsymbol{E}_d(\boldsymbol{r}, t)$ which at large distances $|\boldsymbol{r}| \gg |\boldsymbol{s}|$ from the emitter can be described by (Jackson 1962)

$$\boldsymbol{E}_d(\boldsymbol{r}, t) = -\frac{1}{c^2}\frac{1}{r}[\ddot{\boldsymbol{p}}(t) - (\boldsymbol{p}(t)\cdot\boldsymbol{e}_\mathrm{r})\boldsymbol{e}_\mathrm{r}]. \tag{18}$$

This leads to the ratio

$$\left|\frac{\boldsymbol{E}_\mathrm{d}}{E_\mathrm{i}}\right| = \frac{1}{r^2}\frac{\omega^4}{c^4}|\alpha(\omega)|^2|\boldsymbol{e}_\mathrm{i} - (\boldsymbol{e}_\mathrm{i}\cdot\boldsymbol{e}_\mathrm{r})\boldsymbol{e}_\mathrm{r}|^2 = \frac{1}{r^2}|f(\Omega)|^2. \tag{19}$$

Without going into details, $|\boldsymbol{e}_\mathrm{i} - (\boldsymbol{e}_\mathrm{i}\cdot\boldsymbol{e}_\mathrm{r})\boldsymbol{e}_\mathrm{r}|^2$ can be expressed by $(1 + \cos^2\theta)$ under the assumption of unpolarized radiation which allows one to average over all polarization directions of the incoming radiation. This delivers the scattering cross section

$$\frac{\mathrm{d}\sigma}{\mathrm{d}\Omega} = |f(\theta, \omega)|^2 = \frac{1}{2}(1 + \cos^2\theta)\frac{\omega^4}{c^4}|\alpha(\omega)|^2 \tag{20}$$

for the scattering of a single electron when it is hit by an electromagnetic wave.

The dependence of the scattering cross section on the frequency of the exciting wave can be best discussed for the following cases (figure 7):

$$\omega \ll \omega_\mathrm{r}: \qquad |\alpha(\omega)|^2 \approx \frac{e^4}{m_\mathrm{e}^2\omega^4} \qquad \text{Rayleigh scattering} \tag{21}$$

which is typical for light scattering,

$$\omega \approx \omega_\mathrm{r}: \qquad |\alpha(\omega)|^2 \approx \frac{e^4}{(m_\mathrm{e}\gamma\omega_\mathrm{r})^2} \qquad \text{Resonance scattering} \tag{22}$$

and

$$\omega \gg \omega_\mathrm{r}: \qquad |\alpha(\omega)|^2 \approx \frac{e^4}{m_\mathrm{e}^2\omega_\mathrm{r}^4} \qquad \text{Thomson scattering.} \tag{23}$$

In the last case, typical for hard x-rays, the frequency of the incoming electromagnetic radiation is so high that the electrons are vibrating out of phase without further frequency dependence. This frequency-independent Thomson cross section can be written as

$$\left(\frac{\mathrm{d}\sigma}{\mathrm{d}\Omega}\right)_{\mathrm{Th}} = f_{\mathrm{Th}}(\theta) = \frac{1}{2}r_{\mathrm{e}}^2(1+\cos^2\theta) \tag{24}$$

using the classical electron radius $r_{\mathrm{e}} = e^2/mc^2 = 2.8 \times 10^{-15}$ m. Therefore, $(\mathrm{d}\sigma/\mathrm{d}\Omega)_{\mathrm{Th}}$ is of the order of 10^{-29} m^2.

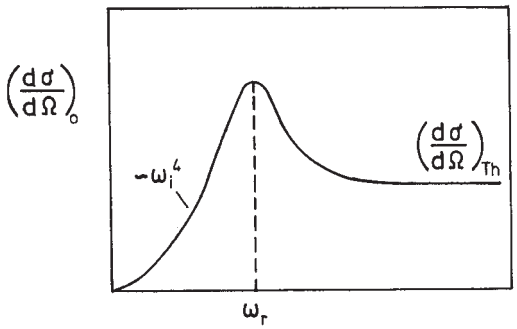

Figure 7. Schematic view of the intrinsic cross section $(\mathrm{d}\sigma/\mathrm{d}\Omega)_0$ for the scattering of electromagnetic radiation in the visible light and x-ray range. ω_{r} is a typical resonance frequency of the scattering system and $(\mathrm{d}\sigma/\mathrm{d}\Omega)_{\mathrm{Th}}$ is the Thomson scattering cross section.

Scattering experiments performed with incident energies E_{i} close to $\hbar\omega_{\mathrm{r}}$ are resonance experiments which allow the enhancement of the scattering response. With modern synchrotron radiation sources such experiments can be easily carried out due to the tunability of the photon energies. Historically, the expression *anomalous dispersion* is used in context with the behaviour of the scattering cross section in this resonance regime. The scattering length $f(\omega)$ itself can be described by adding a complex anomalous scattering length $f'(\omega)+\mathrm{i}f''(\omega)$ to the frequency-independent Thomson part f_{Th}:

$$f(\omega) = f_{\mathrm{Th}} + f'(\omega) + \mathrm{i}f''(\omega). \tag{25}$$

This frequency dependence opens a possibility for the determination of the scattering phase $\Phi(\omega)$

$$f(\omega) = |f(\omega)|\,\mathrm{e}^{\mathrm{i}\Phi(\omega)} \tag{26}$$

which is not possible from (8). For details see, for instance, Materlik *et al* (1994).

3. Scattering of x-rays by an atom

If two electrons at the positions $\mathbf{0}$ and $\boldsymbol{r}_{\mathrm{c}}$ are excited by an incoming electromagnetic wave the phase differences of the scattered waves have to be taken into account. Figure 8 shows the path difference of the scattered waves for such a situation. The phase difference is given by

$$\begin{aligned}\frac{2\pi}{\lambda_{\mathrm{i}}} \times \text{path difference} &= \frac{2\pi}{\lambda_{\mathrm{i}}}\frac{1}{k_{\mathrm{i}}}(\boldsymbol{k}_{\mathrm{i}} - \boldsymbol{k}_{\mathrm{f}})\cdot\boldsymbol{r}_{\mathrm{c}} \\ &= (\boldsymbol{k}_{\mathrm{i}} - \boldsymbol{k}_{\mathrm{f}})\cdot\boldsymbol{r}_{\mathrm{c}} \\ &= \boldsymbol{Q}\cdot\boldsymbol{r}_{c}\end{aligned} \tag{27}$$

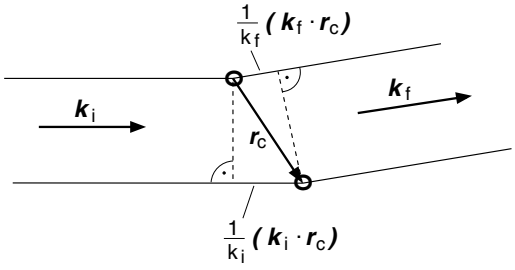

Figure 8. Path difference of waves scattered at the positions **0** and r_c.

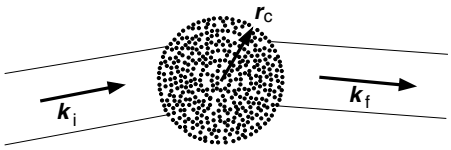

Figure 9. Schematic view of the scattering by the electron distribution of an atom.

using $k_i = k_f = 2\pi/\lambda_i$. Therefore, the scattering amplitude depends on the scattering vector $\boldsymbol{Q}$ and the locations of the electrons, and is obtained by phase-correct addition of both partial waves.

In general, the nucleus in an atom is surrounded by a spatial distribution of electrons, which can be described by a local electron density $n_e(\boldsymbol{r})$ within the atomic volume V. For this discussion, x-ray scattering in the frame of Thomson scattering with $\omega \gg \omega_r$ is assumed.

The scattering amplitudes of all electrons have to be added up using the correct phase shifts, (27), leading to the atomic structure factor $f_j(\boldsymbol{Q})$ by

$$f_j(\boldsymbol{Q}) = \int_V \mathrm{d}V\, n_e(\boldsymbol{r})\, \mathrm{e}^{\mathrm{i}\boldsymbol{Q}\cdot\boldsymbol{r}}. \tag{28}$$

For forward scattering with $\boldsymbol{Q} = 0$ no phase difference occurs and, thus, $f_j(0) = \int_V \mathrm{d}V\, n_e(\boldsymbol{r}) = Z$ with Z being the total number of electrons in the atom. Equation (28) can also be read as the Fourier transform of the spatial electron density distribution $n_e(\boldsymbol{r})$. Due to this spatial distribution of the shell electrons there is always a $\boldsymbol{Q}$ dependence of the x-ray scattering as a footprint of the size and form of the distribution. Figure 10 demonstrates this behaviour for different ions. The obvious Q dependence is absent for neutron scattering experiments, since the nucleus appears as a *point source* on the scale of the thermal neutron wavelengths.

However, for neutron scattering, a Q dependence occurs for the magnetic scattering where the magnetic moment caused by unpaired electrons couples to the magnetic moment of the neutron. Normally, only a few electron orbits in the outer shell of the atom will contribute to the magnetic moment. Therefore, the magnetic scattering form factor for neutrons is not identical to the electronic form factor for x-rays.

4. Scattering from crystals

4.1. Diffraction geometry of crystal lattices

When the atoms are arranged in a crystal lattice the well known idea of Bragg (1913) can be used to understand the scattering intensity distribution. The incoming waves are *reflected* at

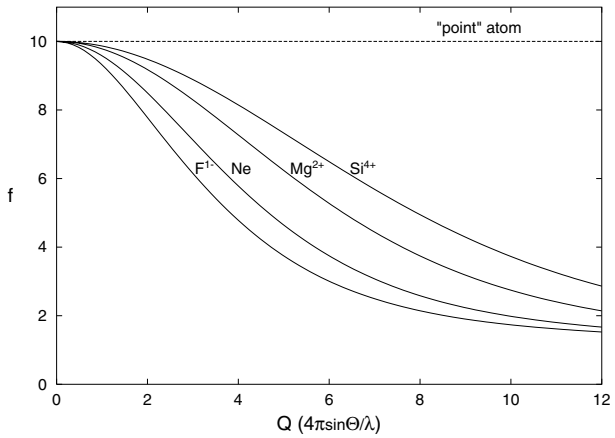

Figure 10. Scattering factors for three ions having a total of ten electrons surrounding the nucleus together with the atomic form factor of neon ($Z = 10$) and a corresponding *point source* with the same charge are shown as functions of Q. The curves are according to data from Hartree–Fock calculations as given in the International Tables for x-ray Crystallography (1974).

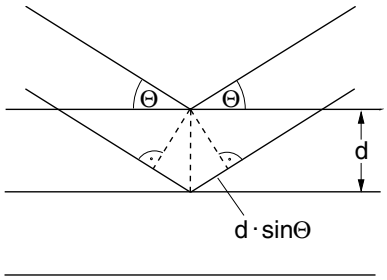

Figure 11. Diffraction geometry with path difference of waves scattered at a crystal lattice.

parallel lattice planes defined by the periodically aligned atoms. Figure 11 demonstrates the path difference between waves being reflected from adjacent planes with spacing d under the Bragg angle θ to be $2d \sin\theta$. Diffraction maxima are visible if this path difference occurs to be an integer multiple of the wavelength,

$$2d \sin\theta = n\lambda_i \qquad \text{Bragg's law.} \tag{29}$$

Bragg's law clearly shows that reflections are only possible for $\lambda \leqslant d$. From the position of the reflections, information on the Bravais lattice type is revealed. In order to analyse a complete crystal structure, additional information on the basis of the structure is necessary. This information can be obtained from the analysis of the intensities of the Bragg maxima, as will be shown later.

4.2. Interference of x-rays at a crystal lattice

Historically, at about the same time von Laue (1940) was following a different approach in order to understand the scattering of x-rays at a crystal lattice. The Bravais lattice has N lattice points n, described by their position vectors $\boldsymbol{r}_n = n_1\boldsymbol{a} + n_2\boldsymbol{b} + n_3\boldsymbol{c}$ with the basis vectors $\boldsymbol{a}$, $\boldsymbol{b}$ and $\boldsymbol{c}$ in real space. For simplicity, only one type of atom is assumed to be present, $f_n = f$.

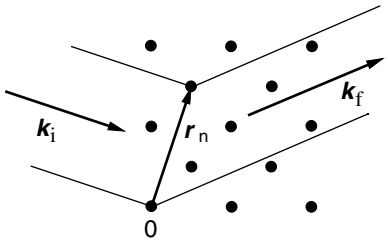

Figure 12. Diffraction geometry with path difference of scattered waves.

The scattered amplitude of such a lattice is then given by the phase-correct addition of all separate scattering contributions

$$\begin{aligned} F'(\boldsymbol{Q}) &= \sum_{n}^{N} f_n \, \mathrm{e}^{\mathrm{i}\boldsymbol{Q}\cdot\boldsymbol{r}_n} \\ &= f(\boldsymbol{Q}) \sum_{n_1,n_2,n_3}^{N} \mathrm{e}^{\mathrm{i}\boldsymbol{Q}(n_1\cdot\boldsymbol{a}+n_2\cdot\boldsymbol{b}+n_3\cdot\boldsymbol{c})} \\ &= f(\boldsymbol{Q})\Big(\sum_{n_1}^{N_1} \mathrm{e}^{\mathrm{i}n_1\boldsymbol{Q}\cdot\boldsymbol{a}}\Big)\Big(\sum_{n_2}^{N_2} \mathrm{e}^{\mathrm{i}n_2\boldsymbol{Q}\cdot\boldsymbol{b}}\Big)\Big(\sum_{n_3}^{N_3} \mathrm{e}^{\mathrm{i}n_3\boldsymbol{Q}\cdot\boldsymbol{c}}\Big). \end{aligned} \tag{30}$$

Here, the lattice sum over N atoms in the crystal is separated into three partial sums over N_1, N_2 and N_3. The sums can be treated as geometric progressions leading to

$$F'(\boldsymbol{Q}) = f(\boldsymbol{Q})\left(\frac{\sin[\frac{1}{2}N_1\boldsymbol{Q}\cdot\boldsymbol{a}]}{\sin[\frac{1}{2}\boldsymbol{Q}\cdot\boldsymbol{a}]}\right)\left(\frac{\sin[\frac{1}{2}N_2\boldsymbol{Q}\cdot\boldsymbol{b}]}{\sin[\frac{1}{2}\boldsymbol{Q}\cdot\boldsymbol{b}]}\right)\left(\frac{\sin[\frac{1}{2}N_3\boldsymbol{Q}\cdot\boldsymbol{c}]}{\sin[\frac{1}{2}\boldsymbol{Q}\cdot\boldsymbol{c}]}\right). \tag{31}$$

The condition for constructive interference with sharp maxima requires that each of the three factors has to be non-zero, individually. This means that $\boldsymbol{Q}$ has to satisfy three equations simultaneously,

$$\boldsymbol{Q}\cdot\boldsymbol{a} = 2\pi h \qquad \boldsymbol{Q}\cdot\boldsymbol{b} = 2\pi k \qquad \text{and} \qquad \boldsymbol{Q}\cdot\boldsymbol{b} = 2\pi l \tag{32}$$

where h, k and l are any set of integers. These conditions are known as *Laue conditions*. In order to identify the solutions of the scattering vector $\boldsymbol{Q}$ that fulfill these conditions the *Ansatz* $\boldsymbol{Q} = h\boldsymbol{A}+k\boldsymbol{B}+l\boldsymbol{C}$ with a new set of basis vector $\boldsymbol{A}$, $\boldsymbol{B}$, $\boldsymbol{C}$ is made. This leads to the relations

$$\boldsymbol{A} = \frac{2\pi}{V_c}(\boldsymbol{b}\times\boldsymbol{c}) \qquad \boldsymbol{B} = \frac{2\pi}{V_c}(\boldsymbol{c}\times\boldsymbol{a}) \qquad \boldsymbol{C} = \frac{2\pi}{V_c}(\boldsymbol{a}\times\boldsymbol{b}) \tag{33}$$

where $V_c = \boldsymbol{a}\cdot(\boldsymbol{b}\times\boldsymbol{c})$ is the volume of a unit cell. The vectors $\boldsymbol{A}$, $\boldsymbol{B}$, $\boldsymbol{C}$ have the dimension of a reciprocal length, therefore the lattice they span is called the reciprocal lattice. In this way, each crystal lattice has two associated lattices, the real lattice with its points $\boldsymbol{r} = n_1\boldsymbol{a}+n_2\boldsymbol{b}+n_3\boldsymbol{c}$ and the reciprocal lattice with its points $\boldsymbol{G} = h\boldsymbol{A}+k\boldsymbol{B}+l\boldsymbol{C}$. Since $\boldsymbol{G}\cdot\boldsymbol{r} = 2\pi\cdot$ integer, the phase factor $\mathrm{e}^{\mathrm{i}\boldsymbol{G}\cdot\boldsymbol{r}}$ equals 1 and, correspondingly, the lattice sum (30) delivers a diffraction maximum for $\boldsymbol{Q} = \boldsymbol{G}$. Therefore, x-ray scattering gives an image of the reciprocal lattice which can be understood as a lattice of reciprocal lattice points in the Fourier space.

4.3. Reciprocal lattice

The role of the reciprocal lattice can be illustrated further with the discussion of the momentum transfers involved in the scattering process. Figure 13 shows the scattering triangle made up by

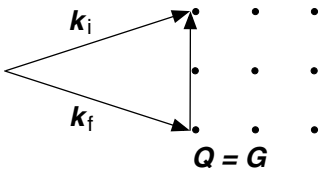

Figure 13. Diffraction geometry with path difference of scattered waves.

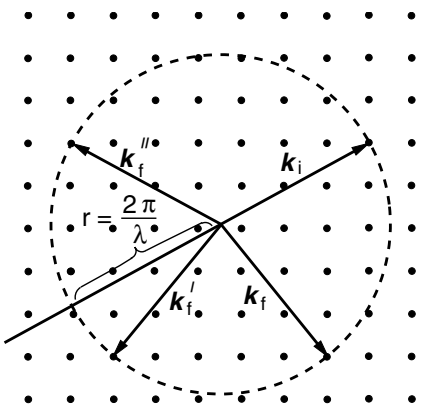

Figure 14. Allowed k_f leading to scattering maxima according to the Ewald construction.

Q, k_i and k_f together with the reciprocal lattice points. There is constructive interference for the indicated case, where the scattering vector Q coincides with the lattice vector G. Therefore,

$$k_i - k_f = Q = G. \tag{34}$$

Multiplying this equation by $\hbar$ delivers

$$\hbar k_f - \hbar k_i = \hbar Q = \hbar G \tag{35}$$

with $\hbar k = \hbar 2\pi/\lambda = h/\lambda = p$ being the momentum. Therefore, (35) being equal to (5) stands for the momentum conservation in the collision process of the x-ray photon and the crystal. $\hbar Q$ is the momentum transfer during the scattering process and $\hbar G$ shows the possible momentum acceptance by the lattice during an elastic process.

This fact was used by P P Ewald for an instructive geometric interpretation of Bragg's law and the prediction of allowed scattering maxima.

In figure 14, k_i shows the direction of the incoming beam and ends at any point of the reciprocal lattice. A sphere of radius $|k_i| = 2\pi/\lambda_i$ around the origin of k_i gives the length of k_f of the scattered beam. Now, any point of the reciprocal lattice on the surface of the sphere defines a diffracted beam, $k_f = k_i - G$.

The unit cell of the reciprocal lattice is the Brillouin zone. Due to translational symmetry it can be shown that all information can be found by investigations of only one Brillouin zone, by the first or any higher one.

4.4. Scattering at a crystal structure

As indicated already earlier, the lattice positions r_n and the basis locations r^α have to be taken into account for the description of the scattering at a crystal structure. Therefore, the complete

scattering amplitude for atoms with atomic form factors $f_\alpha(\boldsymbol{Q})$ in a crystal structure is given by

$$\begin{aligned} F'(\boldsymbol{Q}) &= \sum_{n,\alpha} f_\alpha(\boldsymbol{Q})\, \mathrm{e}^{\mathrm{i}\boldsymbol{Q}\cdot(\boldsymbol{r}_n+\boldsymbol{r}^\alpha)} \\ &= \sum_n \left(\sum_\alpha f_\alpha(\boldsymbol{Q})\, \mathrm{e}^{\mathrm{i}\boldsymbol{Q}\cdot\boldsymbol{r}^\alpha} \right) \mathrm{e}^{\mathrm{i}\boldsymbol{Q}\cdot\boldsymbol{r}_\mathrm{n}} \\ &= \sum_n F(\boldsymbol{Q})\, \mathrm{e}^{\mathrm{i}\boldsymbol{Q}\cdot\boldsymbol{r}_\mathrm{n}} \end{aligned} \tag{36}$$

with the structure amplitude

$$F(\boldsymbol{Q}) = \sum_\alpha f_\alpha(\boldsymbol{Q})\, \mathrm{e}^{\mathrm{i}\boldsymbol{Q}\cdot\boldsymbol{r}^\alpha} \tag{37}$$

which describes the scattering of a unit cell. The structure amplitude causes constructive and destructive interference and can be a complex quantity.

Therefore, the positions and the intensities of the Bragg maxima have to be observed for a complete structural analysis.

4.5. Scattering by an ensemble

In the treatment of the scattering process so far one has assumed a weak interaction between the probe and the scattering system. The scattered intensity is small compared to the primary intensity. There is no interaction between the scattered and the primary wave. Multiple scattering is neglected, and the primary wave is essentially unchanged on its path through the sample. The discussion is carried out within the *kinematic approximation*.

The complete amplitude $F'(\boldsymbol{Q})$ of the scattered wave is then obtained by phase correct superposition of all partial waves originating in the case of x-ray scattering from the electrons with density $n_\mathrm{e}(\boldsymbol{r})$ of the sample

$$F'(\boldsymbol{Q}) = \int_\mathrm{sample} \mathrm{d}^3 r\, n_\mathrm{e}(\boldsymbol{r})\, \mathrm{e}^{\mathrm{i}\boldsymbol{Q}\cdot\boldsymbol{r}}. \tag{38}$$

The measured intensity I is

$$I \propto S(\boldsymbol{Q}) = F'(\boldsymbol{Q}) \cdot F'^*(\boldsymbol{Q}) = |F'(\boldsymbol{Q})|^2. \tag{39}$$

This leads to

$$S(\boldsymbol{Q}) = \frac{1}{N} \left| \int_\mathrm{sample} \mathrm{d}^3\boldsymbol{r}\, n_\mathrm{e}(\boldsymbol{r})\, \mathrm{e}^{\mathrm{i}\boldsymbol{Q}\cdot\boldsymbol{r}} \right|^2 = \frac{1}{N} |\tilde{n}_\mathrm{e}(\boldsymbol{Q})|^2 \tag{40}$$

which shows that the scattering function is determined by the Fourier transform $|\tilde{n}_\mathrm{e}(\boldsymbol{Q})|$ of the electron density distribution $n_\mathrm{e}(\boldsymbol{r})$ in the sample.

In principle, the electron density distribution $n_\mathrm{e}(\boldsymbol{r})$ can then be determined from the experimentally obtained $S(\boldsymbol{Q})$ by back transformation leading to the positions of the chemical elements in the sample. However, such measurements of $S(\boldsymbol{Q})$ can only be performed in a finite $\boldsymbol{Q}$-range with finite resolution $\Delta\boldsymbol{Q}$. This is equivalent to an ensemble average $\langle\rangle_{v_\mathrm{s}}$ on many sample pieces of volume $v_\mathrm{s} = (2\pi/\Delta Q)^3$. This problem becomes serious when instead of perfect periodically ordered systems less ordered ones like alloys or liquids are analysed. Additionally, there is the *phase problem* of the structure analysis, already mentioned in the context of (26), which provides only the magnitude but not the phase Φ of $\tilde{n}_\mathrm{e}(\boldsymbol{Q}) \equiv |\tilde{n}_\mathrm{e}(\boldsymbol{Q})|\, \mathrm{e}^{\mathrm{i}\Phi}$. Therefore, generally speaking one starts with a model assumption for the electron density distribution $n_\mathrm{e}(\boldsymbol{r})$ for the calculation of the scattering function $S_m(\boldsymbol{Q})$, which then is compared

with $S(\boldsymbol{Q})$, the measured one and improved by refinement. Figure 15 shows schematically the procedure of such a structure analysis. Here, it is assumed that the sample with N atoms contains N_μ atoms of the chemical element μ at positions $\boldsymbol{r}_\mu^m$ indicated by the occupation numbers σ_μ^m, being 1 or 0 if the site is occupied or empty, respectively.

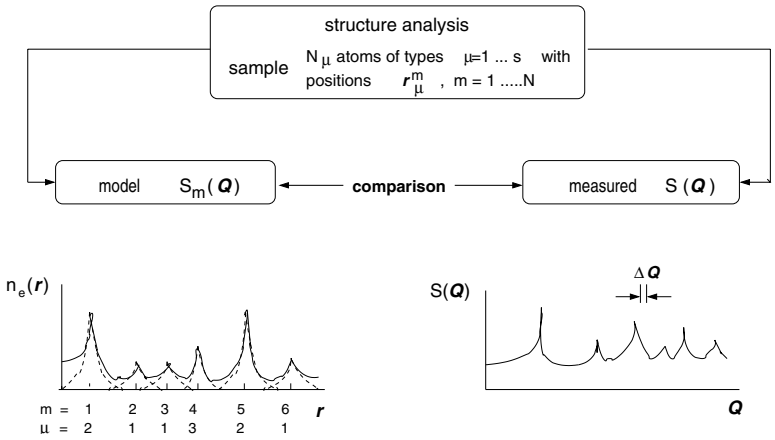

Figure 15. Principle of the structure analysis with comparison of the measured scattering function $S(\boldsymbol{Q})$ with a suited model function $S_m(\boldsymbol{Q})$.

In this way most details of the structure of a sample can be obtained. For further illustration of the structure analysis a few simple cases will be discussed in this scheme.

4.6. Scattering by a monoatomic ideal crystal

Figure 16 shows a simple monoatomic ideal crystal with perfect periodic electron density. The scattering function is obtained by the square of the Fourier transform of the density. It shows a series of δ-functions, which give the Bragg reflection intensities. From their positions the locations of the reciprocal lattice points and, thus, the size and form of the unit cell of the crystal is obtained. The integrated intensities of the Bragg maxima

$$\int_{\boldsymbol{Q}\approx\boldsymbol{G}_{hkl}} S(\boldsymbol{Q})\,\mathrm{d}^3Q = |f(\boldsymbol{G}_{hkl})|^2 \tag{41}$$

deliver the atomic structure factors and, thus, the local electron distribution at the sites of the periodically arranged atoms. Ideally, there is no scattering intensity between the reflections due to destructive interference of the scattered waves.

4.7. Scattering by an ideal crystal with z atoms per unit cell

For an ideal crystal with $z = 2$ atoms per unit cell, figure 17 shows again the electron distribution along one lattice direction and the scattering function calculated on this basis. There are again δ-functions showing the positions of the reciprocal lattice; however, in this case the envelope function determining the integrated intensities of the Bragg maxima leads to the structure amplitude which is known from (37) and which depends on the electron distribution in a unit cell.

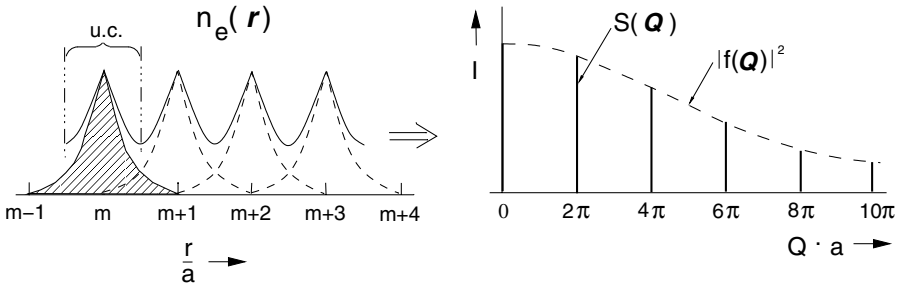

Figure 16. Schematic electron density distribution in real space for a monoatomic ideal crystal along one lattice direction (left-hand side) with the hatch area of a single atom and the scattering function calculated on this basis (right-hand side). The dashed curve indicates the scattering function of a single atom (following Schilling 1992).

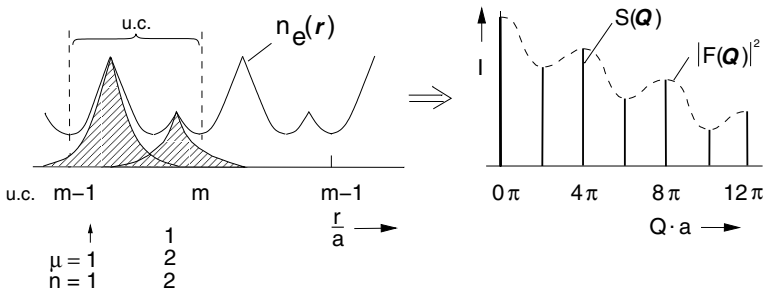

Figure 17. Schematic electron density distribution in real space for a two atomic ideal crystal along one lattice direction (left-hand side) with the hatched areas of the two atomic sorts (μ_1) and (μ_2) and the scattering function calculated on this basis (right-hand side). The dashed curve indicates the square of the structure factor (following Schilling 1992).

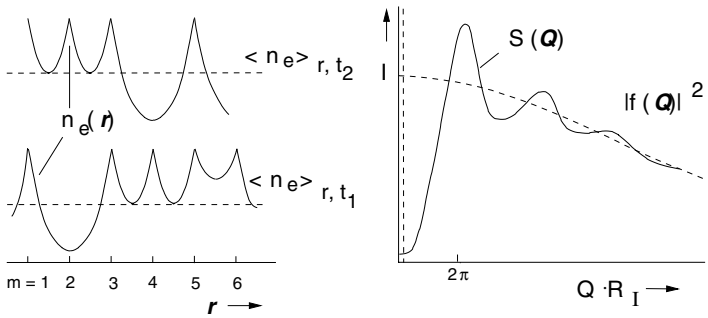

Figure 18. Schematic electron density distribution for certain times of a monoatomic liquid (left-hand side) and its scattering function (right-hand side) (following Schilling 1992).

4.8. Scattering by a monoatomic liquid

Following along this line, it is straightforward to deal also with disordered systems like a monoatomic liquid. It is only necessary to look at the electron density distribution at different times (figure 18). Since the atoms are at different positions at different times during time evolution, the elastic x-ray scattering experiment will average over a series of atomic distributions and deliver only statistical information about the distance distributions in the liquid.

The scattering function (figure 18) exhibits a characteristic structure but no Bragg maxima. At large momentum transfers $\boldsymbol{Q}$ it follows essentially the squared atomic form factor law. This diffuse scattering at large $\boldsymbol{Q}$ represents only the Fourier transform of the electron distribution of single atoms. There are intensity oscillations visible at the positions $Q \approx 2\pi/R_{\mathrm{I}}$ given by the averaged nearest-neighbour distances R_{I}. At small values of Q, the scattering function approaches the value of the isothermal compressibility determined by the macroscopic density fluctuations. The average density of the atoms $\langle n_{\mathrm{e}} \rangle$ leads to a Bragg maxima $\delta(Q = 0)$ in the forward direction. The scattering function can be written as

$$S(\boldsymbol{Q} = \frac{|f(\boldsymbol{Q})|^2}{N} \left\langle \left| \sum_m^N \mathrm{e}^{\mathrm{i}\boldsymbol{Q}\cdot\boldsymbol{r}_m} \right|^2 \right\rangle_{t,V_s}$$
$$= |f(\boldsymbol{Q})|^2 \left\langle \sum_{l=1}^{N-1} \mathrm{e}^{\mathrm{i}\boldsymbol{Q}\cdot(\boldsymbol{r}^m - \boldsymbol{r}^{m+l})} \right\rangle_m \equiv |f(\boldsymbol{Q})|^2 \tilde{g}(\boldsymbol{Q}) \tag{42}$$

with $\tilde{g}(\boldsymbol{Q})$ being the Fourier transform of the pair-correlation function $g(\boldsymbol{R})$ since the double sum in (42) can be written as an average sum over the distances $\boldsymbol{R} = \boldsymbol{r}^m - \boldsymbol{r}^{m+l}$. Here, the pair-correlation function,

$$g(\boldsymbol{R}) = \left\langle \sum_{l=0}^{N-1} \delta(\boldsymbol{R} - \boldsymbol{R}^l) \right\rangle_m \tag{43}$$

describes the probability of starting from any atom in the sample and finding another atom at the distance R^l per volume element. In an isotropic liquid, g is a function of $|\boldsymbol{R}|$ and, thus, $\tilde{g}$ is a function of $|\boldsymbol{Q}|$.

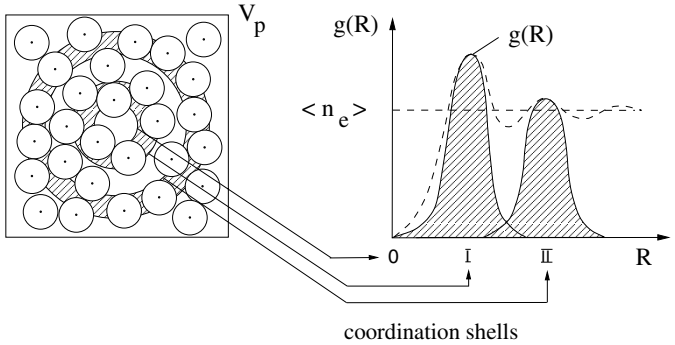

Figure 19. Schematic view of the pair correlation function.

Figure 19 shows the pair correlation function together with a schematic view of the atomic arrangement in the liquid. Since the atoms do not penetrate each other, $g(R \to 0) = 0$. At certain distances R^l, there are maxima of $g(R)$ describing so-called coordination shells (I, II etc) At large Q, $g(R)$ becomes constant and equals the average density $\langle n_{\mathrm{e}} \rangle$ in the liquid.

The ideas presented here are also applicable to amorphous solids.

4.9. Temperature dependance of the scattered intensity

So far, in the discussion of the scattering profiles of the crystalline structures the temperature effect has been neglected. However, the atoms, respectively the electrons, are not at rest, and lattice vibrations exist. There are thermal displacements which can be described as $\boldsymbol{u}(t) = \boldsymbol{u}\cos\omega t$ with $\omega = 10^{12-14}$ Hz. Therefore, the actual positions of the atoms are

$\boldsymbol{r}(t) = \boldsymbol{r}_n + \boldsymbol{u}(t)$. For the calculation of the scattering function a time average has to be performed.

$$F_n(\boldsymbol{Q}) \sim \langle \mathrm{e}^{\mathrm{i}\boldsymbol{Q}\cdot(\boldsymbol{r}_n+\boldsymbol{u}(t))}\rangle_t \sim \mathrm{e}^{\mathrm{i}\boldsymbol{Q}\cdot\boldsymbol{r}_n}\langle \mathrm{e}^{\mathrm{i}\boldsymbol{Q}\cdot\boldsymbol{u}(t)}\rangle_t. \tag{44}$$

It can be shown that for cubic crystals this leads to a reduction of the intensity of a Bragg maximum,

$$I = I_0\,\mathrm{e}^{-\frac{1}{3}\langle u^2\rangle Q^2} = I_0\,\mathrm{e}^{-2W} \tag{45}$$

where e^{-2W} is the Debye–Waller factor (see Warren 1969).

In the high-temperature approximation of a harmonic oscillator, $\langle u^2\rangle = 3k_\mathrm{B}T/M\omega^2$ holds for the mean-square displacement of the atoms. The reduction of the intensity increases with Q^2 (figure 20). The missing intensity is scattered inelastically and visible between the reflections as thermal diffuse scattering (TDS) containing the information on the atomic movements (see the article by Burkel this volume). Because of the ω^{-2}-dependance, the acoustic modes contribute more to the TDS than the optic modes.

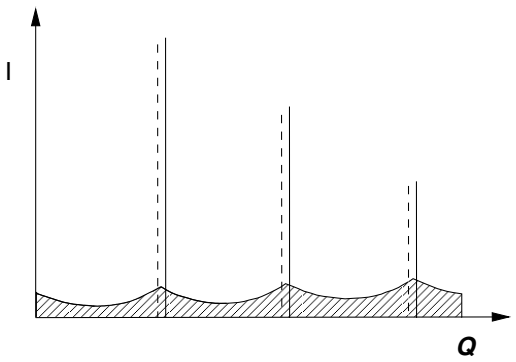

Figure 20. Schematic view of the temperature effect on the scattering intensity distribution.

5. Coherent and incoherent scattering

The scattering cross section for a system with many identical atoms can be written as given in (30). However, even if these are chemically identical atoms there can be different scattering lengths f_μ, for instance in the case of neutrons due to different isotopes or nuclear spins. For a total random arrangement with no correlations assumed, the scattering cross section can be written as

$$\frac{\mathrm{d}\sigma}{\mathrm{d}\Omega} \propto \sum_{n,m} f_m^*(\boldsymbol{Q})\, f_n(\boldsymbol{Q})\, \mathrm{e}^{\mathrm{i}\boldsymbol{Q}\cdot(\boldsymbol{r}_n-\boldsymbol{r}_m)}. \tag{46}$$

The different isotopes μ are statistically distributed with concentration $c_\mu = N_\mu/N$ within the sample. It holds that

$$\bar{f}(\boldsymbol{Q}) = \sum_\mu c_\mu f_\mu(\boldsymbol{Q}) \qquad \text{and} \qquad \overline{|f(\boldsymbol{Q})|^2} = \sum_\mu c_\mu |f_\mu(\boldsymbol{Q})|^2. \tag{47}$$

This leads to

$$\begin{aligned}\overline{f_m^*(\boldsymbol{Q})\, f_n(\boldsymbol{Q})} &= |\overline{f}(\boldsymbol{Q})|^2(1-\delta_{nm}) + \overline{|f(\boldsymbol{Q})|^2}\delta_{nm} \\ &= |\overline{f}(\boldsymbol{Q})|^2 + [\overline{|f(\boldsymbol{Q})|^2} - |\overline{f}(\boldsymbol{Q})|^2]\delta_{nm} \\ &= |\overline{f}(\boldsymbol{Q})|^2 + \overline{|f(\boldsymbol{Q}) - \bar{f}(\boldsymbol{Q})|^2}\delta_{nm}.\end{aligned} \tag{48}$$

Therefore, the scattering function reads as

$$\frac{\mathrm{d}\sigma}{\mathrm{d}\Omega} \sim |f(\boldsymbol{Q})|^2 \cdot S'(\boldsymbol{Q}) + \overline{|\bar{f}(\boldsymbol{Q}) - f(\boldsymbol{Q})|^2} = \left(\frac{\mathrm{d}\sigma}{\mathrm{d}\Omega}\right)_{\mathrm{coh}} + \left(\frac{\mathrm{d}\sigma}{\mathrm{d}\Omega}\right)_{\mathrm{inc}} \tag{49}$$

with the coherent part $(\mathrm{d}\sigma/\mathrm{d}\Omega)_{\mathrm{coh}}$ and the incoherent part $(\mathrm{d}\sigma/\mathrm{d}\Omega)_{\mathrm{inc}}$ of the scattering function.

The first coherent part contains the interference effects and describes scattering from a system with identical atoms $f(\boldsymbol{Q}) = \overline{f}(\boldsymbol{Q})$, in which case the scattering amplitudes are added and then squared. The second or incoherent part does not contain interference effects, and the scattering occurs as of independent scatterers with $f(\boldsymbol{Q}) = \overline{f(\boldsymbol{Q}) - \overline{f}(\boldsymbol{Q})}$. Therefore, the different scattering intensities are added resulting in a weak Q dependance of the scattering intensity. In x-ray scattering, the first part shows the structure as discussed before, whereas the second part with its diffuse scattering reveals disorder effects of the structure as far as the disorder is point-like and uncorrelated.

6. Inelastic scattering

So far, the discussion of the scattering phenomena has been restricted to elastic scattering experiments. However, besides the already mentioned lattice vibrations, there are a variety of other excitations possible in condensed matter.

A typical x-ray excitation spectrum for condensed matter is shown schematically in figure 21. The elastic line at zero energy transfer is indicated as well. The lattice and molecular vibrations have typical energies up to several hundred meV. In the low-eV regime electron–hole pair creation is detectable. Plasmon excitations are correlated with energies around 5 to 20 eV. Core shell excitations require drastically higher energy transfers.

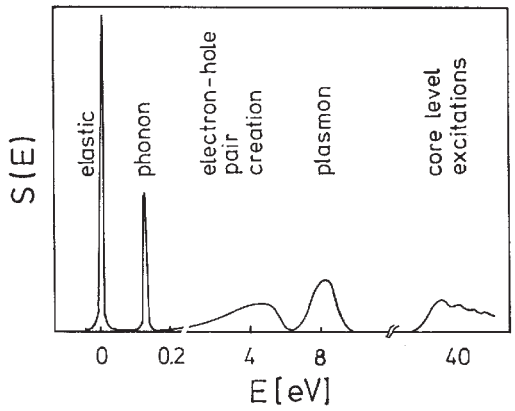

Figure 21. Typical x-ray excitation profile in condensed matter, drawn schematically as a function of the excitation energy. It shows contributions due to elastic scattering, phonon scattering, electron-hole pair creation and plasmonic and core level excitations.

The general scattering experiment follows still the same layout as already sketched in figure 4, only this time energy transfers $E = \hbar\omega \equiv E_{\mathrm{i}} - E_{\mathrm{f}}$ are also resolved. This permits the observation of scattering contributions with changed energy due to inelastic scattering. In this discussion, the transferred energy is still smaller than the photon energy ($E \ll E_{\mathrm{i}}$) and (7) is valid. For the interpretation of inelastic scattering experiments, the double differential scattering cross section $\mathrm{d}^2\sigma/\mathrm{d}\Omega\,\mathrm{d}\omega_{\mathrm{f}}$ and the scattering function $S(\boldsymbol{Q}, \omega)$ from (7) have to be discussed.

The scattering function can be investigated in various modifications. A basic representation for a many-body system of particles at the positions $\boldsymbol{r}_j$ with discrete initial and final states Υ_i and Υ_f is expressed according to Fermi's 'golden rule' by

$$S(\boldsymbol{Q},\omega)=\sum_{\Upsilon_\mathrm{i},\Upsilon_\mathrm{f}}\left|\left\langle\Upsilon_\mathrm{f}\left|\sum_j \mathrm{e}^{\mathrm{i}\boldsymbol{Q}\cdot\boldsymbol{r}_j}\right|\Upsilon_\mathrm{i}\right\rangle\right|^2\delta(\hbar\omega+E_{\Upsilon_\mathrm{f}}-E_{\Upsilon_\mathrm{i}}). \tag{50}$$

The phase of the scattering amplitude is described by $\mathrm{e}^{\mathrm{i}\boldsymbol{Q}\boldsymbol{r}_j}$. The matrix elements contain the probabilities for excitations from the initial to the final states and the delta function gives the information about the corresponding frequency. According to (50), the scattering amplitudes from the different scatterers are added and then squared. This leads to an interference between the scattering amplitudes.

A sophisticated representation of the scattering function was derived by Van Hove (1954),

$$S(\boldsymbol{Q},\omega)=\frac{1}{2\pi}\int \mathrm{d}t\,\mathrm{e}^{-\mathrm{i}\omega t}\left\langle\Upsilon_\mathrm{i}\left|\sum_{\mathrm{j,j'}}\mathrm{e}^{-\mathrm{i}\boldsymbol{Q}\cdot\boldsymbol{r}_\mathrm{j}(\mathrm{t})}\,\mathrm{e}^{\mathrm{i}\boldsymbol{Q}\cdot\boldsymbol{r}_\mathrm{j}(0)}\right|\Upsilon_\mathrm{i}\right\rangle. \tag{51}$$

It describes the correlations of the scattering phases of the particles at positions $\boldsymbol{r}_j(t)$ at different times t. In the classical limit it represents essentially the Fourier transform in time of the density correlation function and gives information on the particle fluctuations in the scattering system in the same initial states Υ_i at different times.

The dependence of the scattering phases on the term $\boldsymbol{Q}\cdot\boldsymbol{r}_j$ can be used for a classification of the scattering process (Platzman 1974). Thereby, the inverse of the transferred momentum $\hbar Q$ has to be compared with a characteristic length ζ_char of the scattering system describing the spatial inhomogeneity. It can be an interparticle distance or a screening length.

For $Q\zeta_\mathrm{char}\ll 1$, there exists interference between the scattering amplitudes from many particles of the system. Consequently, mainly the collective behaviour of the particles will be detectable. Therefore, collective motions of the scattering system like phonons, magnons or plasmons can be observed if, in addition, the transferred energy is in the characteristic frequency range of these excitations.

For $Q\zeta_\mathrm{char}\gg 1$, the interference of the scattering amplitudes is negligible and the scattering contributions of different particles are independent. Therefore, single-particle properties are observed, such as, for example, Compton scattering (Platzman 1974) in the case of photon interaction with an electron system, if the photon energy is large compared to the binding energy of the electron.

In the intermediate ranges $Q\zeta_\mathrm{char}\approx 1$, both collective and single-particle properties are visible.

The scattering function (50) is often transformed to representations that are more suitable to describe important physical properties of a particular system.

For the study of collective excitations, the response of a system to the incident and scattered photons can also be expressed by the imaginary part or, in other words, by the dissipative part of the dynamic susceptibility $\chi(\boldsymbol{Q},\omega)$,

$$S(\boldsymbol{Q},\omega)=-\frac{1}{\pi}\frac{1}{1-\mathrm{e}^{-\beta\hbar\omega}}\mathrm{Im}\,\chi(\boldsymbol{Q},\omega) \tag{52}$$

with $\beta=1/k_\mathrm{B}T$.

For the special application to an electron gas with density N the dielectric function $\varepsilon(\boldsymbol{Q},\omega)$ is usually used in the scattering function (Pines and Noziéres 1966),

$$S(\boldsymbol{Q},\omega)=\frac{\hbar Q^2}{4\pi^2e^2N}\frac{1}{1-\mathrm{e}^{-\beta\hbar\omega}}\mathrm{Im}\left[\frac{-1}{\varepsilon(\boldsymbol{Q},\omega)}\right] \tag{53}$$

where Im $[-1/\varepsilon(\boldsymbol{Q},\omega)]$ is the macroscopic energy loss function describing the response of the electron gas.

Thus, inelastic scattering with synchrotron radiation can access a broad spectrum of single-particle and collective excitations.

In a complete discussion of the inelastic scattering it is import to include both contributions, the coherent and the incoherent parts. Therefore, the double differential cross section has to be written in the form

$$\frac{\mathrm{d}\sigma}{\mathrm{d}\Omega\,\mathrm{d}\omega} = \left(\frac{\mathrm{d}\sigma}{\mathrm{d}\Omega\,\mathrm{d}\omega}\right)_{\mathrm{coh}} S_{\mathrm{coh}}(\boldsymbol{Q},\omega) + \left(\frac{\mathrm{d}\sigma}{\mathrm{d}\Omega\,\mathrm{d}\omega}\right)_{\mathrm{inc}} S_{\mathrm{inc}}(\boldsymbol{Q},\omega) \tag{54}$$

coherent part	incoherent part
$\Downarrow$	$\Downarrow$
interference effects	no interference effects
$\Downarrow$	$\Downarrow$
collective properties	single-particle properties
Fourier transform in space and time of pair-correlation function	Fourier transform in space and time of self-correlation function

The comments below (54) indicate how the coherent and the incoherent parts lead to the determination of the single-particle and the collective properties from the corresponding correlation functions.

So far, the discussion of the interaction of x-ray radiation with the electrons in the sample has been restricted to the Thomson scattering cross section, as introduced in (24). However, in the scattering process the electrons in the sample which are accelerated by the incident field give rise to electric and magnetic dipole reradiation. The Thomson term considers only the electric part. In order to take both contributions into account, the double differential cross section can be written using an expanded scattering function $S'(Q,\omega)$ as (Platzmann and Tzoar 1970)

$$\frac{\mathrm{d}^2\sigma}{\mathrm{d}\Omega\,\mathrm{d}\omega_{\mathrm{f}}} = r_0^2 \cdot S'(\boldsymbol{Q},\omega) = r_0^2 \cdot \sum_{\Upsilon_{\mathrm{i,f}}} \left| \langle \Upsilon_{\mathrm{f}} \left| \sum_j \boldsymbol{M}_j \, \mathrm{e}^{\mathrm{i}\boldsymbol{Q}\boldsymbol{r}_j} \right| \Upsilon_{\mathrm{i}} \rangle \right|^2 \delta(E_{\mathrm{f}} - E_{\mathrm{i}} - \omega). \tag{55}$$

$\boldsymbol{M}_j$ is the amplitude for the scattering from a single electron with position $\boldsymbol{r}_j$ and spin $\boldsymbol{\sigma}_j$. In a simplified approach with only leading terms, the amplitude $\boldsymbol{M}_j$ is written as

$$\boldsymbol{M}_j = \boldsymbol{A} + \mathrm{i}\boldsymbol{B}\boldsymbol{\sigma}_j$$

with

$$\boldsymbol{A} = \boldsymbol{e}_{\mathrm{i}} \cdot \boldsymbol{e}_{\mathrm{f}}$$

and

$$\boldsymbol{B} = -\hbar\omega_{\mathrm{i}}/mc^2[(\boldsymbol{e}_{\mathrm{i}} \cdot \boldsymbol{e}_{\mathrm{f}}(\hat{k}_{\mathrm{i}} \times \hat{k}_{\mathrm{f}}) - 1/2(\hat{Q}\,\hat{Q})(\boldsymbol{e}_{\mathrm{i}} \times \boldsymbol{e}_{\mathrm{f}}) - \hat{Q} \times (\hat{Q} \times \boldsymbol{e}_{\mathrm{i}} \times \boldsymbol{e}_{\mathrm{f}}).$$

$\hat{k}_{\mathrm{i}}, \hat{k}_{\mathrm{f}}$ are unit wavevectors (Blume 1985).

The first part of the amplitude $\boldsymbol{M}_j$ describes the charge scattering through the Thomson scattering term and leads to (7) and (24), as discussed so far. The second part gives the spin-dependent part of the scattering amplitude. Its magnitude is about $\hbar\omega_{\mathrm{i}}/mc^2 \approx 10^{-2}$.

This small spin-dependent part can be observed due to the fact that the magnitude of the Thomson contribution can be varied and even be extinguished experimentally by an appropriate selection of the polarization vectors. There is also an interference term between the spin-dependent and the spin-independent terms. By using linearly or circularly polarized photons,

for instance, from an asymmetric wiggler, these contributions can be distinguished, and the magnetic response functions of different systems can be studied.

Understanding of magnetic phenomena requires a knowledge of the whole magnetic excitation spectrum. Magnetism in condensed matter is produced by unpaired electrons. Strong exchange interactions lead to collective excitations, magnons, which merge after a strong dispersion into a broad particle–hole continuum. The excitation energies are as high as several electronvolts.

Due to the small magnitude of the magnetic scattering term the scattering cross section has, including form factors, a ratio of about 4×10^{-6} between charge and magnetic scattering for x-rays in the kiloelectronvolt range. This means that the study of magnons with inelastic x-ray scattering needs high photon energies and even more intense sources than presently available.

7. Conclusions

This short discussion of basic properties of scattering experiments will be useful for the following contributions which specialize on inelastic scattering aspects.

Acknowledgments

Thanks goes to Ch Benkißer and U Ponkratz for their assistance in the preparation of the figures.

References

Blume M 1985 *J. Appl. Phys.* **57** 3615
Bonifacio R, De Salvo L, Pierini P, Piovella N and Pelligrini C 1994 *Phys. Rev. Lett.* **73** 70
Bragg W L 1913 *Proc. Cambridge Phil. Soc.* **17** 43
Brinkmann R, Materlik G, Rossbach J and Wagner A (eds) 1997 Conceptional design of a 500 GeV $e^+ e^-$ linear colider with integrated laser facility *Report* DESY-1997-048/EFCA-1997-182, Hamburg
Freund H P and Neil G R 1999 *Proc. IEEE* **87** 782
International Tables for X-ray Crystallography 1974 vol IV (Birmingham: Kynoch)
Jackson J D 1962 *Classical Electrodynamics* (New York: Wiley)
Lovesey S W 1986 *Theory of Neutron Scattering from Condensed Matter* vol I, II (Oxford: Clarendon)
Materlik G, Sparks C J and Fischer K (eds) 1994 *Resonant Anomalous X-ray Scattering—Theory and Applications* (Amsterdam: Elsevier Science)
Pines D and Nozières P 1966 *The Theory of Quantum Liquids* (New York: Benjamin)
Platzmann P M 1974 *Elementary Excitations in Solids, Molecules and Atoms Part A (Nato Advanced Study Institutes B)* ed J T Devreese, A B Kunz and T C Collins (New York: Plenum)
Platzmann P M and Tzoar N 1970 *Phys. Rev.* B **2** 9 3556
Saldin E L, Schneidmiller and Yurkov M V 1995 *Phys. Rep.* **260** 187
——2000 *The Physics of Free Electron Lasers* (Berlin: Springer)
Schilling W 1992 *Synchrotronstrahlung zur Erforschung kondensierter Materie* (Jüelich: IFF-Ferienkurs Forschungszentrum)
van Hove L 1954 *Phys. Rev.* **95** 249
von Laue M 1940 *Röntgenstrahlinterferenzen* (Frankfurt a M: Akademische Verlagsgesellschaft)
Warren B E 1969 *X-ray Diffraction* (Reading, MA: Addison-Wesley)